# Novel applications of objective measures in cochlear implants

Dong, Y.

# Chapter 6

# Detection of Translocation of Cochlear Implant Electrode Arrays by Intracochlear Impedance Measurements

Yu Dong, Jeroen J. Briaire, Michael Siebrecht, H. Christiaan Stronks and Johan H. M. Frijns

Ear and Hearing (2021; 42; 1397–1404)

# Abstract

**Objectives：** Misplacement of the electrode array is associated with impaired speech perception in patients with cochlear implants (CIs). Translocation of the electrode array is the most common misplacement. When a CI is translocated, it crosses the basilar membrane from the scala tympani into the scala vestibuli. The position of the implant can be determined on a postoperative CT scan. However, such a scan is not obtained routinely after CI insertion in many hospitals, due to radiation exposure and processing time. Previous studies have shown that impedance measures might provide information on the placement of the electrode arrays. The electrode impedance was measured by dividing the plateau voltage at the end of the first phase of the pulse by the injected current. The access resistance was calculated using the so-called access voltage at the first sampled time point after the start of the pulse divided by the injected current. In our study, we obtained the electrode impedance and the access resistance to detect electrode translocations using electrical field imaging. We have investigated how reliably these two measurements can detect electrode translocation, and which method performed best.

**Design：** We calculated the electrode impedances and access resistances using electrical field imaging recordings from 100 HiFocus Mid-Scala CI (Advanced Bionics, Sylmar, CA) recipients. We estimated the normal values of these two measurements as the baselines of the implant placed in the cochlea without translocation. Next, we calculated the maximal electrode impedance deviation and the maximal access-resistance deviation from the respective baselines as predictors of translocation. We classified these two predictors as translocations or nontranslocations based on the bootstrap sampling method and receiver operating characteristics curves analysis. The accuracy could be calculated by comparing those predictive results to a gold standard, namely the clinical CT scans. To determine which measurement more accurately detected translocation, the difference between the accuracies of the two measurements was calculated.

**Results:** Using the bootstrap sampling method and receiver operating characteristics–based optimized threshold criteria, the 95% confidence intervals of the accuracies of translocation

detections ranged from 77.8% to 82.1% and from 89.5% to 91.2% for the electrode impedance and access resistance, respectively. The accuracies of the maximal access-resistance deviations were significantly larger than that of the maximal electrode impedance deviations. The location of the translocation as predicted by the access resistance was significantly correlated with the result derived from the CT scans. In contrast, no significant correlation was observed for the electrode impedance.

**Conclusions：** Both the electrode impedance and access resistance proved reliable metrics to detect translocations for HiFocus Mid-Scala electrode arrays. The access resistance had, however, significantly better accuracy and it also reliably detected the electrode-location of translocations. The electrode impedance did not correlate significantly with the location of translocation. Measuring the access resistance is, therefore, the recommended method to detect electrode-array translocations. These measures can provide prompt feedback for surgeons after insertion, improving their surgical skills, and ultimately reducing the number of translocations. In the future, such measurements may allow near-real-time monitoring of the electrode array during insertion, helping to avoid translocations.

**Keywords:** Cochlear implants, Sensorineural hearing loss, Deafness, Electrode translocation, Electrode impedance, Access resistance, Electrical field imaging

# 6.1 Introduction

A cochlear implant (CI) is an intracochlear device that can restore hearing through direct electrical stimulation of the auditory nerve. Severely-to-profoundly deaf people with sensorineural hearing loss can benefit from a CI (Hughes 2012). However, speech perception outcomes show large variability (Firszt et al. 2004; Holden et al. 2013). An important factor determining speech perception is the placement of the electrode array. Misplacement is typically associated with poorer speech performance (Aschendorff et al. 2007; Finley & Skinner 2009; Gifford et al. 2013; Holden et al. 2013; Wanna et al. 2014; Carlson et al. 2015; O'Connell et al. 2016). The shift of an electrode array from the scala tympani to the scala vestibuli through the

basilar membrane is called a translocation (Finley & Skinner 2009; Holden et al. 2013; O'Connell et al. 2016; Dhanasingh & Jolly 2017). Translocation is the most common type of electrode misplacement in patients with CIs, although the incidence rates reported in the literature vary widely, from as little as 4% to as high as 54% in a couple of research groups across different electrode array types (Holden et al. 2013; Wanna et al. 2014; O'Connell et al. 2016; Dhanasingh & Jolly 2017). It is possible to detect translocations on a CT scan (Wanna et al. 2014). However, radiology is not routinely applied because it requires additional work, and leads to radiation exposure of patients. As a consequence, insertion trauma often goes unnoticed. In addition, radiological measures cannot be easily applied to monitor the insertion during surgery. For these reasons, an alternative tool is needed to detect translocations.

One promising alternative is the use of impedance measurements. Impedance is a measure of the resistance of current flow through a medium. Clinically, electrode impedance (clinical impedance) recordings are supported by the state-of-the-art cochlear implant systems from all the current implant providers, e.g., Advanced Bionics, Med-EL, Cochlear Ltd and Oticon Medical (Hughes 2012; Dang et al. 2015). Earlier studies found that electrode impedance can be indicative of the endocochlear environment adjacent to the electrode contacts (Agnew et al. 1983; Suesserman & Spelman 1993; Saunders et al. 2002; Tykocinski et al. 2005; Giardina et al. 2017). However, they have not yet been deployed for the detection of electrode translocations. Electrode impedances can be indicative of the endocochlear environment adjacent to the electrode contacts (Agnew et al. 1983; Saunders et al. 2002; Tykocinski et al. 2005; Giardina et al. 2017). Translocation presents the electrode contacts with new medium and tissue characteristics. Due to the differences in resistivity of different tissues and media (Frijns et al. 1995), the impedance in the vicinity of the translocation might also change.

Two different impedance measurements can potentially detect electrode translocation, i.e., the electrode impedance and the access resistance. These two metrics can be obtained using electrical field imaging (EFI) method (Vanpoucke et al. 2004a; Hughes 2012). EFI involves the recording of a matrix of voltages across the measuring electrodes. EFIs are usually recorded by

stimulating one electrode and recording the voltage back with all electrodes. These are commonly converted to impedances to reflect a conductivity map of the intracochlear tissues by dividing the voltages by the current injected by the stimulating electrode (Vanpoucke et al. 2004a; Mens 2007). When translocation occurs, this conductivity map may change accordingly. Within this EFI impedance matrix, the off-diagonal impedances reflect the resistive component of the tissue and fluid between the stimulating and return electrodes (Clark et al. 2003; Vanpoucke et al. 2004b; Hughes 2012). The decay of the off-diagonal impedance as a function of distance has been modeled with various decay functions because exponential decays are not necessarily constant from the base toward the apex in the cochlea (e.g., Vanpoucke et al. 2004a, b; 2012).

The diagonal impedances within the EFI matrix refer to the electrode impedances where the stimulating electrode was also used as the recording contact. In earlier studies, these diagonals were omitted since the higher potential densities in the vicinity of the electrodes cannot be appropriately described by an exponential decay (e.g., Jolly et al. 1996; Briaire et al. 2000; Mens et al. 2003; Vanpoucke et al. 2004a). Nevertheless, these electrode impedances may be useful for detecting electrode translocation due to the access resistance component which can presumably increase when electrode translocation occurs. (Clark et al. 2003; Vanpoucke et al. 2004b; Hughes 2012). Specifically, the access resistance depends on the size and type of metal in the electrode contact and lead wire, and the resistivity of the surrounding fluid and tissue in cochlear implants (e.g., perilymph, fibrous tissue, bone; Clark et al. 2003; Tykocinski et al. 2005). The access resistance can be extracted by simulating the electrode impedance as an electrical circuit model as shown in Figure 6.1. This model combines a serial resistor (representing the access resistance, $R_a$) with the polarization impedance ($Z_P$) of the electrode-electrolyte interface, which is modeled as a parallel circuit with polarization resistance ($R_f$) and capacitance ($C_w$). In this model, the $R_a$ arises from the resistivity of the bulk-surrounding of the intracochlear electrode array; the polarization impedance ($Z_p$) is determined by the electrochemical electrode-electrolyte interface between the charged metal electrode surface and the surrounding fluid or tissue. $C_w$ results from the capacitive effect of the interface between the stimulating electrode

and surrounding tissue medium, whereas $R_f$ is the charge transfer resistance (Clark & Richter 2004;; Vanpoucke et al. 2004b; Tykocinski et al. 2005; Hughes 2012). The access resistance component in Figure 6.1 would change upon translocation, which can place the electrode contact in a different tissue environment. As a consequence, the access resistance near the translocation site will deviate from the normal value, and hence may be an indicator of translocation. Given that the electrode impedance contains the access resistance component, we hypothesized the electrode impedance may also be feasible for detecting electrode translocations. However, how a translocation affects the polarization impedance ($Z_P$) component of the electrode impedance is still uncertain. This polarization component may contaminate the effect of the electrode impedances in reflecting translocation. Thus, we further hypothesized that the access resistance ($R_a$) could be more capable of detecting translocations than the electrode impedance. This study aimed to assess whether the electrode impedance (the combination of the $R_a$ and $Z_P$) and the $R_a$ can be used to detect electrode translocation, and which metric is more viable.

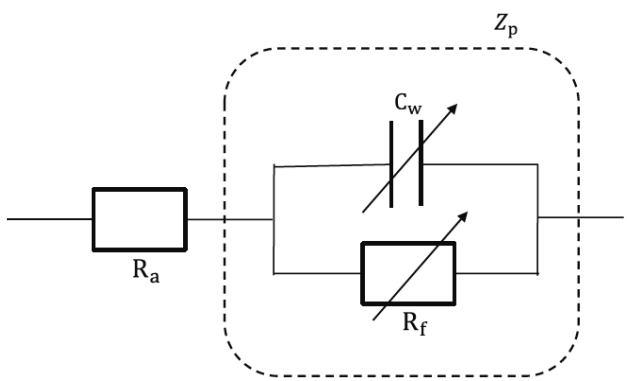


*Fig. 6.1 Electrical circuit diagram for contact impedance (Vanpoucke et al. 2004b; Hughes 2012). $R_a$ represents the access resistance (electrode contact, electrode lead wire, fluid/tissue medium). $C_w$ represents the capacitance of the electrode-tissue interface between the electrode surface and the surrounding fluid or tissue. $R_f$ represents potential faradic resistance that transfers charges via chemical reactions. $Z_p$ represents the polarization impedance at the electrode-electrolyte interface by modelling the $C_w$ and $R_f$ in parallel.*

# 6.2 MATERIAL AND METHODS

### 6.2.1 Subjects

The electrode impedances and the access resistances used in the present retrospective study were obtained from 106 patients who consecutively received a HiRes90K Mid-Scala electrode array (Advanced Bionics, Sylmar, CA) between June 2012 and September 2018. This electrode array consists of 16 platinum contacts with 0.9 mm spacing (1 to 16 in apical-to-basal order). Preoperative and postoperative multi-slice computed tomography scans (Aquilion; Toshiba Medical Systems, Otowara, Japan) were performed according to the standard protocol for cochlear implant patients at the Leiden University Medical Centre (van der Jagt et al. 2017a). According to the CT image, we excluded patients with pre-operative characteristics that may affect the electrode array trajectory, such as a single case of cochlear ossifications, and two patients who underwent a re-implantation. Patients with high noisy impedance measurements (i.e., the electrode impedance was larger than 25 kOhm) (n = 3) were excluded. Therefore, a total of 100 patients were included in the analysis (Table 6.1).

***TABLE 6.1. Patient demographics***

| | |
|---|---|
| Number of Patients | 100 |
| Gender (n) | |
| Male | 41 |
| Female | 56 |
| Mean age ± SD (years) | 41 ±26 |
| Etiology (n) | |
| Meningitis | 4 |
| Meniere's disease | 1 |
| Otosclerosis | 0 |
| Congenital/Hereditary | 39 |
| Other/Unknown | 56 |

### 6.2.2 Data recording

The EFI recordings were performed immediately after the insertion of the electrode array just after the round window closure using the electrical field imaging and modeling (EFIM) tool from Advanced Bionics (for details, see Vanpoucke et al. 2004b). In brief, all 16 contacts were sequentially recorded from apex to base using monopolar recording mode. The reference electrode was the implant casing in the mastoid bone. The CI processor has a built-in amplifier with an analog-to-digital converter that operates at a sample rate of 56 kHz. Each electrode contact is driven by a separate current source, and a blocking capacitor is present in the internal device electronics to prevent DC stimulation. Current passed through the blocking capacitor and the lead wire to the contact. At a recording contact, the difference of potentials between this contact and the reference electrode was recorded. In EFI, each time the intracochlear potential was measured at all contacts with biphasic pulses with an amplitude of 40 μA lasting 66.45 μs per phase. The diagonal voltages in EFI were used to calculate the electrode impedances and the access resistances.

To calculate the electrode impedances expressed in Ohm units, the potentials recorded at the end of the first phase of the pulse were divided by the injected current. Figure 6.2A shows an example of an EFI for a patient (S73) with translocation and an example of an EFI for a patient (S10) without translocation is given in Figure 6.2B. Only the electrode impedances marked by circles were used for analysis.

The approach used to extract access resistance was described by Tykocinski et al. (2005) and Giardina et al. (2017). In brief, the CI electrode-electrolyte interface was modeled as shown in Figure 6.1. The response waveform to a stimulus pulse includes two sources of voltage increase consistent with this model: an immediate jump in voltage from the frequency-independent resistive elements between the contact and the ground (i.e., access resistance), and a slowly increasing limb voltage representing a charge accumulation at the electrode-electrolyte interface (polarization voltage). The access resistances were calculated using the access voltage at the first sampled time point divided by the injected current pulse amplitude.

### 6.2.3 Translocation detection from CT imaging

We used the results from CT images as the gold standard. The pre- and postoperative CT images were used to visually assess them side by side to confirm if electrode translocation occurred, as described in detail by Van der Jagt et al. (2017b). According to their CT image outcome, we identified 25 of the 100 patients included in the present study in whom the array was translocated and the other 75 patients in whom it was contained within the scala tympani.

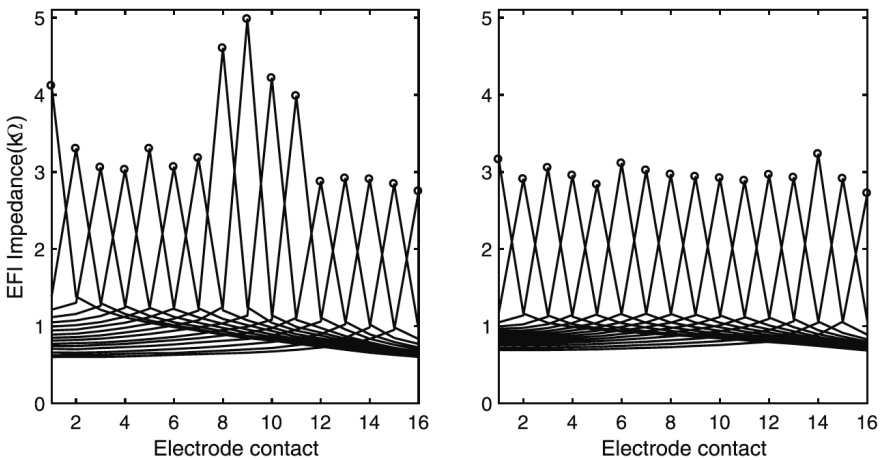


*Fig. 6.2 Two typical EFI maps recorded with biphasic pulses 40-µA, lasting 66.45 µs per phase. Contact 1 (16) is the most apical (basal) one. Each of the 16 spread curves shows the intracochlear impedance profile generated when a single contact is stimulated. A, EFI map with a translocation (S73). B, EFI map without a translocation (S10). The electrode impedances (circles) were used for further analysis.*

### 6.2.4 Analysis

#### 6.2.4.1 Translocation detection from electrode impedances and access resistances

We performed three steps to generate the predictors of translocation based on the electrode impedances. We hypothesized that translocation changes the electrode impedances of nearby contacts. To calculate this deviation, we fitted the baselines of the 16 electrode impedances with a straight line to obtain a measure of normal baseline impedances (in Fig. 6.3, green solid lines).

To this end, we used robust linear regression with the bisquare weighting function (robustfit, MATLAB, Mathworks 2016a, Natick, MA) to minimize the influence of any outliers on the baseline fit. The outliers are expected to include those electrode impedances near a translocation. With these baseline values, we obtained the deviations of the 16 electrode impedances by calculating their distances from the electrode impedance to their baseline. We used the maximal EFI electrode impedance deviation of these 16 deviations to identify the most likely candidates for electrode translocation (in Fig. 6.3C, blue solid lines).

In the same manner, we used robust fitting to obtain the baseline of the 16 access resistances. The distances from the access resistances to this baseline were calculated, and the maximal access-resistance deviation of these 16 values (in Fig. 6.3, blue solid lines) was used to identify the most likely candidate for electrode translocation.

#### 6.2.4.2 Estimating the thresholds and accuracies of the electrode impedance deviations and the access resistance deviations for predicting a translocation

To estimate the thresholds and the accuracies of translocation detections, we used bootstrapping by randomly selecting subgroups of 80% of the patients that were used to predict the translocations in the remaining 20% of patients. To improve reliability, 500 random selections were performed using the bootstrapping method. This sampling method has been described by Harrell et al. (1996). Receiver operating characteristics (ROC) curves were generated to graphically display the performance (Schisterman et al. 2005; Brown & Davis 2006). The weight of a false positive and false negative result was identical. The ROC curves were used to estimate the thresholds for the maximal electrode impedance deviations and the maximal access-resistance deviations using the CT image as the gold standard. The thresholds were used as criteria for translocation detection of the remaining 20% of patients. In the latter group, translocations were determined (true positives) as well as non-translocations (true negatives). Similarly, false positives (type Ⅰ error) and false negatives (type Ⅱ error) were determined. The accuracies refer to the percentage of the true positives and the true negatives for each measure

relative to the total number of samples (i.e., the remaining 20% of patients) of the electrode impedance and the access resistance can be calculated for the remaining 20%.

The confidence intervals of the accuracies and thresholds of the two measures from the 500 selections were calculated. To determine which measurement was better at detecting translocation, we compared the accuracies of the two measurements using the Wilcoxon rank-sum test.

#### 6.2.4.3 Predicting the location of translocations using the electrode impedance and the access resistance

We further investigated if the two measurements were able to predict the location of translocations. To this end, we defined the electrode contact where the maximal electrode impedance deviation and the maximal access-resistance deviation appeared as the location of translocation. We correlated the location of translocation (true positive cases) by the two measurements with the contact where translocation occurred according to CT images using Pearson's correlation coefficient.

# 6.3 RESULTS

Figure 6.3 illustrates the principle of translocation detection with EFI. Figures 6.3A and B show two three-dimensional (3D) reconstructions of 2 patients' cochleas with and without a translocation obtained using a custom-made MATLAB software routine (Siebrecht et al. 2019). In the translocation case, the electrode array pierces the basilar membrane from the scala tympani to the scala vestibuli near electrode 8 (Fig. 6.3A). The outcomes of the maximal electrode impedances and the maximal access resistances of the cochlea with a translocation are shown in Figures 6.3C and E. In these two panels, the maximal electrode impedance deviation and the maximal access-resistance deviation exceed the optimal threshold near electrode 8, and hence accurately reflect the translocation. Similarly, Figure 6.3B shows the 3D reconstruction of the

cochlea without translocation, in which the whole electrode array is contained within the scala tympani. Figures 6.3D and F show the corresponding electrode impedances and access

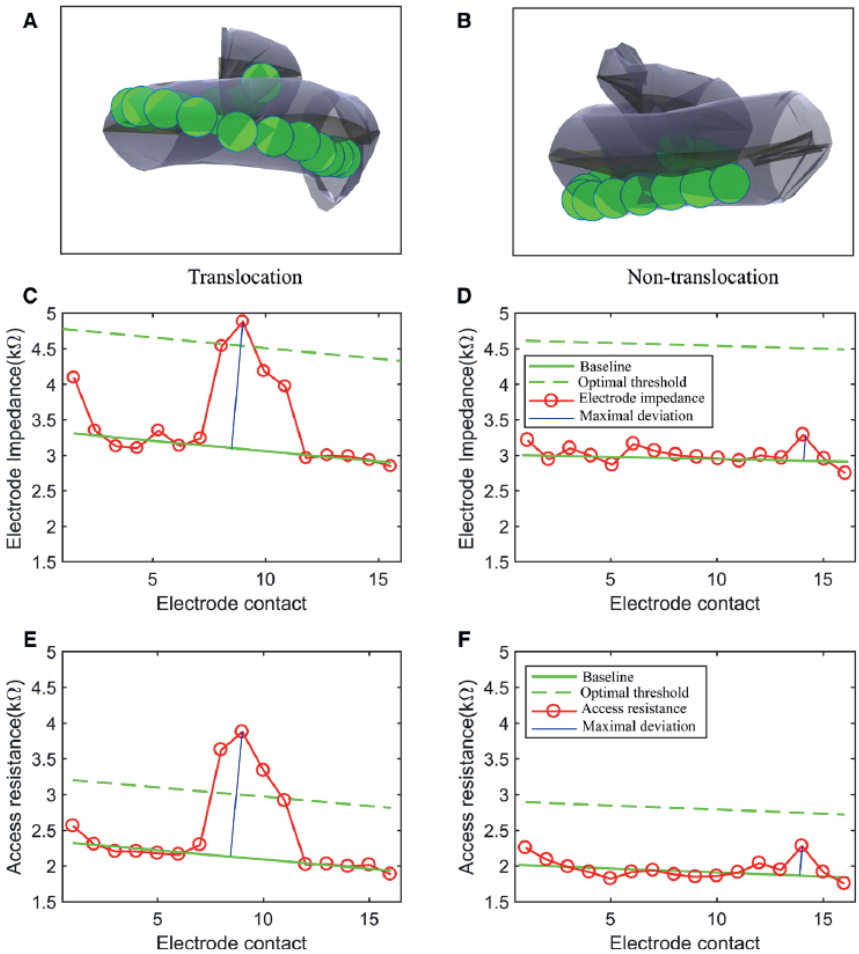


*Fig. 6.3 Examples of translocation (A, C, E; S73) and non-translocation (B, D, F; S10). A and B, 3D reconstructions based on CI scan image of a cochlea with (A) and without a translocation (B), respectively. C and D, the electrode impedances corresponding to the two examples. E and F, the respective access resistances of the two examples. The dashed green lines in C, D, E, and F indicate the optimal thresholds derived from the ROC analysis for predicting the occurrence of a translocation.*

resistances, respectively. The maximal electrode impedance deviation and the maximal access-resistance deviation stay below the optimal thresholds, indicating an absence of translocation.

The optimal threshold in each of these two examples refers to the medians of thresholds for predicting translocation obtained from 500 random elections (described below). In these two examples, the detection of translocation is consistent with the outcomes based on the CT-scan images.

We investigated the thresholds and the accuracies of translocation detection with the electrode impedance and access resistance from 500 random selections. The median value of the electrode impedance was 1.26 kOhm (CI95%: 1.21–1.36 kOhm) and the median accuracy was 78.7% (CI95%: 77.8%–82.1%). The median access resistance was 0.85 kOhm (CI95%: 0.84–0.86 kOhm) and the median accuracy was 90% (CI95%: 89.5%–91.2%). The accuracy of the access resistance is significantly larger than that of the electrode impedance using the Wilcoxon rank-sum test ($p < 0.0001$).

***TABLE 6.2. Detection of translocations with the electrode impedance and the access resistance using median***

| | True positive | True negative | False positive Type Ⅰ error | False negative Type Ⅱ error | Accuracy |
|---|---|---|---|---|---|
| Electrode impedance | 21 | 62 | 13 | 4 | 83% |
| Access resistance | 25 | 66 | 9 | 0 | 91% |

*The CT image outcomes were used as the gold standard: 25 patients with a translocation, and 75 patients without a translocation; Total = 100; Accuracy = (true positive + true negative)/Total.*

The medians of thresholds for the maximal electrode impedance deviations and the maximal access-resistance deviations were used as the optimal thresholds to detect translocations of all the patients. Accordingly, 21 true positives and 62 true negatives were found using the maximal electrode impedance deviations as shown in Table 6.2. The maximal access-resistance deviations resulted in 25 true positives and 66 true negatives. The accuracies of the two measurements were 83% and 91%, respectively.

We further investigated if the two measurements were capable of detecting the location of the

translocation, using only the true-positive cases. For the electrode impedance measurement, the median of translocation contacts of the 21 true positives (with median deviation) was 10 ± 2.6 and ranged from electrode contact 1 to 13. We found that the translocation locations did not significantly correlate with the translocation contacts according to CT imaging using Pearson's correlation coefficient (r = 0.21, p = 0.31) (Fig. 6.4A). For the access resistance measurement, the median of translocation contacts of the 25 true positives (with median deviation) was 9 ± 1.2 and ranged from contact 6 to 15 which was significantly correlated with the results based on CT imaging (r = 0.79, p < 0.001) (Fig. 6.4B).

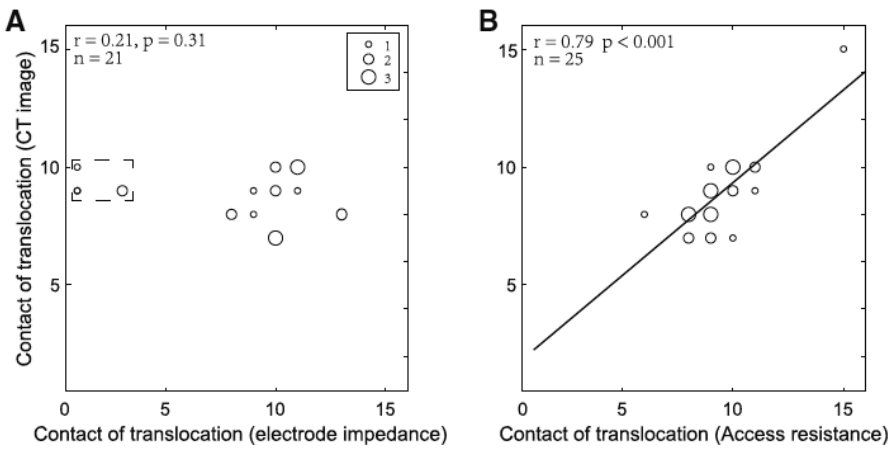


*Fig. 6.4 Scatterplots showing the correlation between the location of translocation from CT image outcomes (y-axis) and the location of translocation from electrode impedance measure (A, y-axis) and the access resistance (B, y-axis). The dashed rectangle indicates the data points that the electrode impedance measure failed to detect the location of translocation.*

# 6.4 DISCUSSION

Electrode-array translocations are detected commonly by analyzing postoperative (cone beam) CT images. Postoperative CT scans are not routinely made in many hospitals. In those hospitals where they are routinely performed after implantation surgery, it is often only after several days following the CI insertion. Hence, often there is no immediate feedback available to the surgeon regarding whether the insertion procedure resulted in translocation of the electrode array. Such

feedback is important, given that the reported incidence rates of translocation in several groups worldwide can be as high as 54% (e.g., O'Connell et al., 2016; Dhanasingh et al. 2017). In the present study, we found that the electrode impedance and the access resistance can both detect translocations, but the access resistance achieved significantly better accuracy. More importantly, only the access resistance was capable of predicting the location of the translocation (Fig. 6.4). These findings are consistent with our hypothesis that access resistance is a more viable predictor of translocation detection. Therefore, we recommend the use of the access resistance as an outcome measure for the detection of translocation, rather than the electrode impedance.

The current study shows that measuring access resistance is a viable, non-invasive method for detecting translocation of a HiFocus Mid-Scala electrode array without the need for a CT scan. Although the access resistance is not a commonly used metric, it can easily be determined in minutes based on EFI recordings. When translocations are detected, the cochlear damage has already been done; at that point in time retracting the electrode array could easily cause additional trauma to patients and is not advised. However, detecting translocation in patients immediately after insertion can potentially benefit surgeons by providing direct feedback. This can help improve their skills for future CI insertions and reduce insertion trauma (Trehan et al. 2015).

Although it is not completely clear how translocation of electrode array occurs, it is assumed that this is affected by the surgical technique, cochlear morphology, and the physical qualities of the array (Wanna et al. 2014; Trehan et al. 2015). In particular, the variability in the morphology of scala tympani, including its height, width, and cross-sectional area, could potentially play an important role in the occurrence of translocation (e.g., Aschendorff et al. 2005; Verbist et al. 2009; Avci et al. 2014). In these studies, the scalae tympani were classified into three different categories according to the variability in the vertical trajectory. The sloping category follows an upward trajectory from the round window without significant downward tendencies. The intermediate category shows a local rise in the vertical direction at the beginning, followed by a gradual decrease from the round window. The rollercoaster category follows a downward trajectory from the round window, changing to upward course between 75° to 120°, hence

generating a dip in the vertical trajectory (e.g., Avci et al. 2014). This rollercoaster category of scala tympani could force the electrode array initially into the downward direction and then into the upward direction. This may lead to trauma to the basilar membrane and translocation into the scala vestibuli at 180° location (e.g., Aschendorff et al. 2005; Verbist et al. 2009; Avci et al. 2014; van der Jagt et al. 2017). The location of translocations in the present study was 170° ± 19° according to the CT image, which was highly consistent with the rollercoaster category.

In this study, we found that the access resistance is a more accurate measure for detecting translocation than the electrode impedance. There are two possible explanations for these differences between the two measures. Tykocinski et al. (2005) proposed a contact impedance model to calculate the different components in CI electrode impedance, as shown in Figure 6.1. According to this model, when a translocation occurs, the most important change will be a change in the medium in the vicinity of the translocation site. This change mainly alters the access resistance, because its value depends on the surrounding medium (Clark et al. 2003; Tykocinski et al. 2005). How a translocation affects other capacitive and faradic resistance components of the electrode impedance is unclear. Hence, these components in the contact impedance model might obscure the effect of the electrode impedances in reflecting translocation, as illustrated by the three circles marked by a dashed rectangle in Fig. 6.4A. This speculation is supported by our observation that the access resistance measure yielded more true positives and fewer false negatives than the electrode impedance, meaning that the access resistance measure can reliably predict the location of translocation but the electrode impedance fails to do so (Fig. 6.4).

It is noteworthy that an increase in the access resistances or the electrode impedances does not necessarily indicate an electrode translocation (i.e., a false positive), because other possible causes could lead to an increase in impedance. For instance, electrode fold-over (Vanpoucke et al. 2012), or tissue, blood, air, or an unknown impurity sticking to the electrode contact during CI insertion might result in a noticeable upward deviation in impedance (Hughes 2012). This could explain the false positives in both the electrode impedance and the access resistance

method in this study. However, we cannot exclude other factors that may have caused the occurrence of false positives. We examined the CT images when our methods yielded false positives or false negatives. Unfortunately, the CT images did not yield any visual clues about the underlying reasons for the occurrence of the observed false negatives and false positives. The limited resolution of the CT images may have been partly responsible for this. Our findings also suggested that the translocation may be detected post-operatively. Note that, as time goes by after the implantation, other factors may result in an increase in impedance, such as ossifications and fibrosis (e.g., Xu et al. 1997; Tykocinski et al. 2001; Hughes 2012). This may lead to false positives. Therefore, the accuracy of the post-operative detection of electrode translocations may decline. Of note, all the patients in the current study received a HiFocus Mid-Scala electrode array where no tip-foldover occurred. Hence, the generalizability to other implant types requires further study.

Previous studies found that electrically evoked compound action potential threshold ratio between the apical and the basal portions could be used to detect a translocation (e.g., Mittmann et al. 2015, 2017). However, the NRT threshold method only yields information whether a translocation has occurred or not, and not about the exact location of the translocation along the electrode array. In contrast, we have found that the access-resistance measurement is a viable method to identify electrode translocation and where it has occurred along the electrode array. The electrically evoked compound action potential threshold ratio method depends on a detectable electrically evoked compound action potential threshold. Since electrically evoked compound action potential thresholds cannot always be determined, e.g., because of progressive degeneration of nerve fibers, the access resistance measurement may be a more feasible tool for detecting translocation in CI recipients.

Preventing intracochlear misplacement during CI insertion is thought to be important for better speech understanding (Usami et al. 2014; Dhanasingh et al. 2017). The influence of electrode translocation on speech perception in CI recipients will be examined in our center. Further, although the present method is not suitable for avoiding translocations, our findings suggest that

this method could theoretically be adapted to deliver real-time impedance measurements during insertion. Such a real-time monitoring system could provide the feedback necessary to assess the intra-cochlear placement of the electrode arrays and guide the surgeon in avoiding translocation of the array and also, perhaps, tip fold-overs. For instance, when the impedance starts changing, potentially indicating that misplacement is about to occur, the surgeon could take proper measures to avoid the misplacement, e.g., adjusting the angle and/or the speed of the insertion. In our center, EFI measurements are routinely performed, but only after CI insertion has been completed. However, we will investigate these possible uses of impedance measurements in the future.

# 6.5 CONCLUSIONS

We found that the electrode impedance and the access resistance can be used to detect electrode translocation immediately after intracochlear insertion without a CT scan. Using the access resistance proved to be a superior metric in terms of accuracy. Therefore, we recommend that access resistance measurements be used to monitor for translocations postoperatively. Our method can potentially be applied intra-operatively and could be extended into a useful tool to prevent or reduce the rate of translocations.

# ACKNOWLEDGMENTS

The first author of the current study is financially supported by the China Scholarship Council. There are no conflicts of interest, financial, or otherwise.

Yu Dong designed and performed experiments, analyzed data and wrote the paper; Jeroen J. Briaire designed experiments and provided critical revision; Michael Siebrecht performed partially data analysis, discussed the results and implications and provided critical revision; H. Christiaan Stronks discussed the results and implications and provided critical revision; Johan H. M. Frijns discussed the results and implications and provided critical revision.

# REFERENCES

Agnew, W. F., Yuen, T. G., McCreery, D. B. (1983). Morphologic changes after prolonged electrical stimulation of the cat's cortex at defined charge densities. Exp Neurol, 79, 397–411.

Aschendorff, A., Kromeier, J., Klenzner, T., & Laszig, R. (2007). Quality Control After Insertion of the Nucleus Contour and Contour Advance Electrode in Adults. Ear and Hearing, 28(Supplement), 75S-79S.

Avci, E., Nauwelaers, T., Lenarz, T., Hamacher, V., & Kral, A. (2014). Variations in microanatomy of the human cochlea. Journal of Comparative Neurology, 522(14), 3245–3261.

Briaire, J. J., & Frijns, J. H. M. (2000). Field patterns in a 3D tapered spiral model of the electrically stimulated cochlea. Hearing Research, 148(1–2), 18–30.

Brown, C. D., & Davis, H. T. (2006). Receiver operating characteristics curves and related decision measures : A tutorial, 80, 24–38.

Carlson, M. L., Driscoll, C. L. W., Gifford, R. H., Service, G. J., Tombers, N. M., Hughes-Borst, B. J., Neff, B. A., & Beatty, C. W. (2015). Implications of Minimizing Trauma During Conventional Cochlear Implantation. Journal of Investigative Dermatology, 135(2), 612–615.

Clark, G., & Richter, C. P. (2004). Cochlear Implants: Fundamentals and Applications. Physics Today, 57(11), 66-67.

Dang, K., Clerc, M., Vandersteen, C., Guevara, N., & Gnansia, D. (2015). In situ validation of a parametric model of electrical field distribution in an implanted cochlea. International IEEE/EMBS Conference on Neural Engineering, NER, 2015-July, 667–670.

Dhanasingh, A., & Jolly, C. (2017). An overview of cochlear implant electrode array designs. Hearing Research, 356, 93–103.

Finley, C. C., & Skinner, M. W. (2009). Role of electrode placement as a contributor to variability in cochlear implant outcomes, 29(7), 920–928.

Firszt, J. B., Holden, L. K., Skinner, M. W., Tobey, E. A., Peterson, A., Gaggl, W., Runge-Samuelson, C. L., & Wackym, P. A. (2004). Recognition of Speech Presented at Soft to Loud Levels by Adult Cochlear Implant Recipients of Three Cochlear Implant Systems. Ear and Hearing, 25(4), 375–387.

Frijns, J. H. M., de Snoo, S. L., & Schoonhoven, R. (1995). Potential distributions and neural excitation patterns in a rotationally symmetric model of the electrically stimulated cochlea. Hearing Research, 87(1–2), 170–186.

Giardina, C. K., Krause, E. S., Koka, K., & Fitzpatrick, D. C. (2017). Impedance Measures during in vitro

Cochlear Implantation predict Array Positioning. IEEE Transactions on Biomedical Engineering, 65(2), 327–335.

Gifford, R. H., Dorman, M. F., Skarzynski, H., Lorens, A., Polak, M., Driscoll, C. L. W., Roland, P., & Buchman, C. A. (2014). Cochlear implantation with hearing preservation yields significant benefit for speech recognition in complex listening environments. 34(4), 413–425.

Harrell, Jr, F. E., Lee, K. L., Mark, D. B. (1996). Multivariable prognostic models: Issues in developing models, evaluating assumptions and adequacy, and measuring and reducing errors. Stat Med, 15, 361–387.

Holden, L. K., Finley, C. C., Firszt, J. B., Holden, T. A., Brenner, C., Potts, L. G., Gotter, B. D., Vanderhoof, S. S., Mispagel, K., Heydebrand, G., & Skinner, M. W. (2013). Factors Affecting Open-Set Word Recognition in Adults With Cochlear Implants. Ear and Hearing, 34(3), 342–360.

Jolly, C. N., Spelman, F. A., Clopton, B. M. (1996). Quadrupolar stimulation for cochlear prostheses: Modeling and experimental data. IEEE Trans Biomed Eng, 43, 857–865.

Mens, L. H. M. (2007). Advances in Cochlear Implant Telemetry: Evoked Neural Responses, Electrical Field Imaging, and Technical Integrity. Trends in Amplification, 11(3), 143–159.

Mittmann, P., Ernst, A., & Todt, I. (2015). Intraoperative Electrophysiologic Variations Caused by the Scalar Position of Cochlear Implant Electrodes. Otology and Neurotology, 36(6), 1010–1014.

Mittmann, P., Todt, I., Ernst, A., Rademacher, G., Mutze, S., Göricke, S., Schlamann, M., Lang, S., Arweiler-Harbeck, D., & Christov, F. (2017). Radiological and NRT-Ratio-Based Estimation of Slim Straight Cochlear Implant Electrode Positions: A Multicenter Study. Annals of Otology, Rhinology and Laryngology, 126(1), 73–78.

Siebrecht, M., Briaire, J. J., & Frijns, J. H. M. Automated Inter-scalar Shift Detection for the HiFocus Mid- Scala from CT scans. In: CIAP 2019.

Hughes, M. L. (2012). Objective Measures in Cochlear Implants. Abingdon, SD: PLURAL PUBLISHING.

O'Connell, B. P., Cakir, A., Hunter, J. B., Francis, D. O., Noble, J. H., Labadie, R. F., Zuniga, G., Dawant, B. M., Rivas, A., & Wanna, G. B. (2016). Electrode Location and Angular Insertion Depth Are Predictors of Audiologic Outcomes in Cochlear Implantation. Otology & Neurotology, 37(8), 1016–1023.

Saunders, E., Cohen, L., Aschendorff, A., Shapiro, W., Knight, M., Stecker, M., Richter, B., Waltzman, S., Tykocinski, M., Roland, T., Laszig, R., & Cowan, R. (2002). Threshold, Comfortable Level and Impedance Changes as a Function of Electrode-Modiolar Distance. Ear and Hearing, 23(1 SUPPL.), 28–40.

Schisterman, E. F., Perkins, N. J., Liu, A., & Bondell, H. (2005). Optimal Cut-point and Its Corresponding Youden Index to Discriminate Individuals Using Pooled Blood Samples, 16(1), 73–81.

Suesserman, M. F., & Spelman, F. A. (1993). Lumped-Parameter Model for In Vivo Cochlear Stimulation. IEEE Transactions on Biomedical Engineering, 40(3), 237–245.

Trehan, A., Barnett-vanes, A., Carty, M. J., & Mcculloch, P. (2015). The impact of feedback of intraoperative technical performance in surgery : a systematic review, 1–5.

Tykocinski, M., Duan, Y., Tabor, B., & Cowan, R. S. (2001). Chronic electrical stimulation of the auditory nerve using high surface area (HiQ) platinum electrodes, 159.

Tykocinski, M., Cohen, L. T., & Cowan, R. S. (2005). Measurement and analysis of access resistance and polarization impedance in cochlear implant recipients. Otology and Neurotology, 26(5), 948–956.

Usami, S. I., Moteki, H., Tsukada, K., Miyagawa, M., Nishio, S. Y., Takumi, Y., Iwasaki, S., Kumakawa, K., Naito, Y., Takahashi, H., Kanda, Y., & Tono, T. (2014). Hearing preservation and clinical outcome of 32 consecutive electric acoustic stimulation (EAS) surgeries. Acta Oto-Laryngologica, 134(7), 717–727.

Van Der Jagt, M. A., Briaire, J. J., Verbist, B. M., & Frijns, J. H. M. (2017a). Comparison of the HiFocus Mid-Scala and HiFocus 1J electrode array: Angular insertion depths and speech perception outcomes. Audiology and Neurotology, 21(5), 316–325.

Jagt, A. M. A. V. Der, Kalkman, R. K., Briaire, J. J., Verbist, B. M., & Frijns, J. H. M. (2017b). Variations in cochlear duct shape revealed on clinical CT images with an automatic tracing method. Scientific Reports, 7(1), 1–9.

Vanpoucke, F., Zarowski, A., Casselman, J., Frijns, J., & Peeters, S. (2004a). The facial nerve canal: an important cochlear conduction path revealed by Clarion electrical field imaging. Otology & Neurotology, 25(3), 282-289.

Vanpoucke, F. J., Zarowski, A. J., & Peeters, S. A. (2004b). Identification of the impedance model of an implanted cochlear prosthesis from intracochlear potential measurements. IEEE Transactions on Biomedical Engineering, 51(12), 2174–2183.

Vanpoucke, F. J., Boermans, P. B. P. B., & Frijns, J. H. (2012). Assessing the placement of a cochlear electrode array by multidimensional scaling. IEEE Transactions on Biomedical Engineering, 59(2), 307–310.

Verbist, B. M., Ferrarini, L., Briaire, J. J., Zarowski, A., Admiraal-Behloul, F., Olofsen, H., Reiber, J. H. C., & Frijns, J. H. M. (2009). Anatomic considerations of cochlear morphology and its implications for insertion trauma in cochlear implant surgery. Otology and Neurotology, 30(4), 471–477.

Wanna, G. B., Noble, J. H., Carlson, M. L., Gifford, R. H., Dietrich, M. S., Haynes, D. S., Dawant, B. M.,

& Labadie, R. F. (2014). Impact of Electrode Design and Surgical Approach on Scalar Location and Cochlear Implant Outcomes. Laryngoscope, 124(S6), S1–S7.

Xu. J, R. K. S., R.E. Millard, G.M. Clark. (1997). Chronic electrical stimulation of the auditory nerve at high stimulus rates: a physiological and histopathological study. Hear Res., 105 (1–2) (1997), pp. 1-29.